Chem Soc Rev

TUTORIAL REVIEW

View Article Online
View Journal | View Issue

Cite this: *Chem. Soc. Rev.*, 2014, 43, 1349

Multifunctional polymer–metal nanocomposites *via* direct chemical reduction by conjugated polymers

Ping Xu,*[ab] Xijiang Han,*[a] Bin Zhang,[a] Yunchen Du[a] and Hsing-Lin Wang*[b]

Received 25th October 2013

DOI: 10.1039/c3cs60380f

www.rsc.org/csr

Noble metal nanoparticles (MNPs) have attracted continuous attention due to their promising applications in chemistry, physics, bioscience, medicine and materials science. As an alternative to conventional solution chemistry routes, MNPs can be directly synthesized through a conjugated polymer (CP) mediated technique utilizing the redox chemistry of CPs to chemically reduce the metal ions and modulate the size, morphology, and structure of the MNPs. The as-prepared multifunctional CP–MNP nanocomposites have shown application potentials as highly sensitive surface enhanced Raman spectroscopy (SERS) substrates, effective heterogeneous catalysts for organic synthesis and electrochemistry, and key components for electronic and sensing devices. In this tutorial review, we begin with a brief introduction to the chemical nature and redox properties of CPs that enable the spontaneous reduction of noble metal ions to form MNPs. We then focus on recent progress in control over the size, morphology and structure of MNPs during the conjugated polymer mediated syntheses of CP–MNP nanocomposites. Finally, we highlight the multifunctional CP–MNP nanocomposites toward their applications in sensing, catalysis, and electronic devices.

Key learning points

(1) Redox chemistry of conjugated polymers that renders the spontaneous chemical reduction of metal ions.
(2) One-step synthesis of metal nanoparticles through a direct conjugated polymer mediated technique.
(3) Size, morphology and structure control of metal nanoparticles during the conjugated polymer mediated synthesis.
(4) Applications of nanocomposites comprising metal nanoparticles and conjugated polymers in sensing, catalysis, and electronics.

1. Introduction

Noble metal nanoparticles (MNPs), such as Pt, Pd, Au, and Ag, have attracted continuous attention due to their promising applications in optical, electronic, sensing, biomedical and energy devices.[1] The properties of MNPs strongly depend on their size, morphology, composition, crystallinity, and surface structures.[2] Thus, various approaches have been developed to control the size and morphology of MNPs through physical, chemical, and even biological methods so as to optimize their properties for specific applications.[3] However, in order to realize anisotropic growth of nanocrystals, most chemical routes require organic solvents and polymer capping agents, which are environmentally unfriendly and cost ineffective. In addition, chemical syntheses are usually limited to one-recipe-one-structure, lacking flexibility in size and morphology control.

Conjugated polymers (CPs), also known as intrinsically conductive polymers, are widely used in various applications due to their conductivity, and optical and electronic properties.[4] Chemical structures of some intensively studied CPs are shown in Fig. 1. The conventional CPs are polyaniline (PANI), polypyrrole (PPy), and polyacetylene (PA) and their derivatives, which have been widely studied primarily due to their intrinsic conductivity and processibility.[5] Other classes of CPs, such as polythiophene (PT) and polyphenylene (PP) and their derivatives, with unique and tunable electronic and optical properties, have shown promise in optoelectronic and luminescence devices.[4] Another important class of materials involving CPs is nanocomposites, which consist of CPs and MNPs; they have been very attractive

[a] *HIT-HAS Laboratory of High-Energy Chemistry and Interdisciplinary Science, Department of Chemistry, Harbin Institute of Technology, Harbin 150001, China. E-mail: pxu@hit.edu.cn, hanxijiang@hit.edu.cn; Fax: +86-451-8641-8750; Tel: +86-451-8641-3702*

[b] *Chemistry Division, Los Alamos National Laboratory, Los Alamos, NM 87545, USA. E-mail: hwang@lanl.gov; Fax: +1-505-667-9944; Tel: +1-505-665-6811*

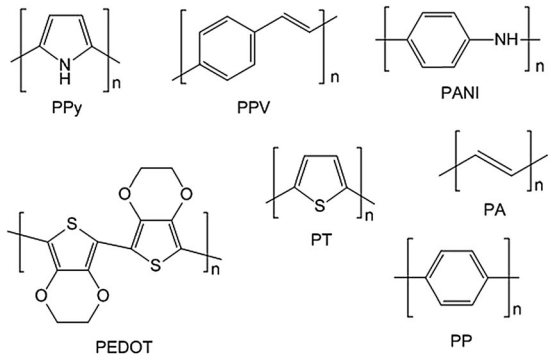

Fig. 1 Molecular structures of extensively studied conjugated polymers.

for various applications, due to the synergetic properties pertaining to the two components.[6] Most fabrication techniques for preparing CP nanocomposites employ electrochemical deposition or electropolymerization routes to allow the formation of such nanocomposites, where MNPs and metal oxide (sulfide) NPs can be immobilized on CPs. Pt, Cu, Zn, Cu_2O and CdS have been successfully fabricated on CP surfaces or embedded in CP matrices through the electrodeposition technique.[7,8] Despite recent advances in fabricating MNPs, it is extremely desirable to have a universal synthetic platform which has delicate control over the size, morphology and structure of MNPs and CPs, so that application potentials of such nanocomposites can be fully realized. In this review, we describe tailoring synthesis of nanostructured metals with a wide range of sizes, structures and morphologies and their applications toward catalysis, sensing, and electronic devices.

It has been recognized that a metal ion having a higher reduction potential (E^0) than a CP, once in contact, can be spontaneously reduced by the CP to form zero-valent metal (Scheme 1a).[9] Electron transfer from CP to metal ions also

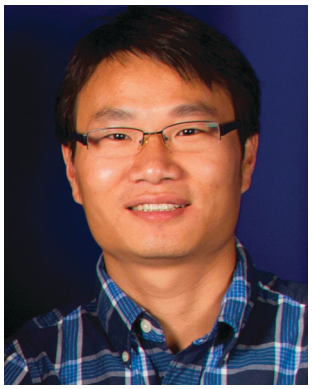

Ping Xu

Ping Xu was born in Zhejiang, China. He received a BS degree in Applied Chemistry (2003) and a PhD degree in Chemical Engineering and Technology (2010) from the Harbin Institute of Technology (HIT). He is now an Associate Professor at HIT. He spent one year as a visiting student and one and a half years as a Director's Postdoctoral Fellow in Dr Wang's group at Los Alamos National Laboratory (LANL). He received the 2011 LANL Small Team Distinguished Performance Award. His current research interests include design and synthesis of nanostructured materials and hybrid materials for applications in surface enhanced Raman spectroscopy, surface plasmon assisted catalysis reactions, and advanced energy devices.

Xijiang Han

Xijiang Han was born in Heilongjiang, China. He received a BS degree in Physical Chemistry (1986) from Nankai University and a PhD degree in Environmental Science and Engineering (2003) from the Harbin Institute of Technology (HIT). He started as an Assistant Professor at Northeastern Agricultural University in 1986 and moved to HIT in 1998. He is now a Professor in the Department of Chemistry at HIT. His research interests include synthesis of nanomaterials for applications in microwave absorption, sensing and photocatalysis.

Bin Zhang

Bin Zhang was born in Harbin, China. She received a MS degree in Electrochemistry (2005) and a PhD degree in Chemical Engineering and Technology (2009) from the Harbin Institute of Technology (HIT). She then started as an Engineer at HIT. Her current research interests include synthesis of high-performance electrode materials and electrocatalysts for energy devices.

Yunchen Du

Yunchen Du was born in Harbin, China. He received his BS degree in Chemistry (2003) and PhD degree in Inorganic Chemistry (2008) from Jilin University. He then started as an Assistant Professor at HIT and was promoted to Associate Professor in 2012. His current research interests include nanoporous and nanostructured materials for applications in heterogeneous catalysis, SERS and microwave absorption.

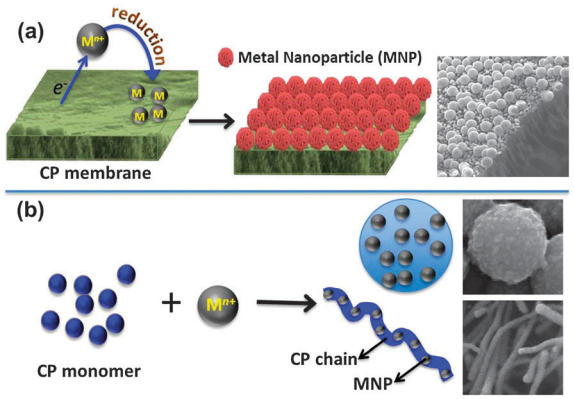

Scheme 1 Schematic illustration of the two reaction pathways to fabricate CP–MNP nanocomposites *via* a direct chemical reduction technique: (a) chemical reduction of metal ions by conjugated polymers and (b) chemical oxidation of monomers by metal salts.

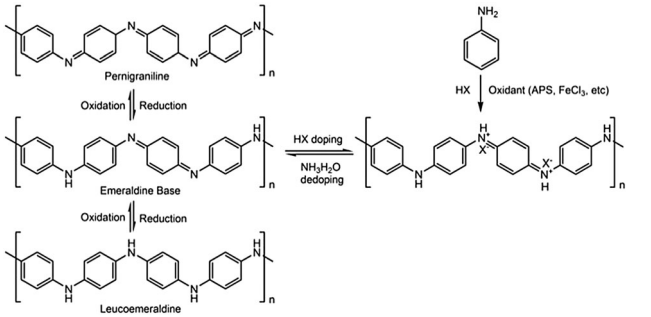

Fig. 2 The synthesis, reversible acid–base, doping–dedoping and oxidation–reduction processes of a representative conjugated polymer, polyaniline (PANI).

results in the oxidation of CP to a higher oxidation state. This synthetic platform utilizes the CP as both the template and reducing agent, without the involvement of any other organic solvents and reducing agents. For example, PANI is one of the most promising CPs for commercial applications due to its facile synthesis, low cost and environmental stability. In the emeraldine base form, PANI becomes electrically conductive when doped with an acid (see Fig. 2).[10] The doping level and thus the electrical conductivity of PANI can be controlled by the pH of the dopant acid solution. Oxidation states of PANI can also be controlled, *via* chemical or electrochemical means, where emeraldine base form can be oxidized to pernigraniline, or reduced to leucoemeraldine. This reversible redox feature renders chemical reduction of metal ions, and the ease of changing the surface chemistry of PANI by the doping process allows morphology and size control of the MNPs through the CP-mediated synthesis. To date, Ag^+, Au^{3+}, Pd^{2+}, and Pt^{2+} ions have been found to be spontaneously reduced by PANI to form zero-valent metals (see Table 1).[11] However, metal ions such as Cu^{2+}, Ni^{2+}, and Zn^{2+}, with lower E^0 than PANI, cannot be spontaneously reduced by PANI, and additional electric field is thus required to reduce these metal ions.[12] PPy, PANI–PPy copolymers, poly(3,4-ethylene dioxythiophene) (PEDOT), poly(phenylene vinylene) (PPV) and several other CPs have also been demonstrated to be able to chemically reduce noble metal ions to zero valent metals.[13–17]

Table 1 Standard reduction potentials of PANI and several metal ions and chemical reduction possibility of metal ions by PANI

	E^0 (V)	ΔE^a (V)	Possibility[b]
PANI	0.70–0.75	—	—
Ag^+/Ag	0.80	0.05	√
Au^{3+}/Au	1.50	0.75	√
Pt^{2+}/Pt	0.755	0.005	√
Pd^{2+}/Pd	0.83	0.08	√
Cu^{2+}/Cu	0.34	−0.41	×
Ni^{2+}/Ni	−0.25	−1.10	×
Zn^{2+}/Zn	−0.76	−1.51	×

[a] ΔE is the reduction potential difference between the metal ions and PANI (using 0.75 V). [b] Possibility here means the spontaneous chemical reduction of metal ions by PANI.

Another aspect in terms of synthesizing polymer–metal nanocomposites *via* the direct CP-mediated route lies in the polymerization of monomers by metal salts ($HAuCl_4$, $Au(ClO_4)_4^-$, $PtCl_4^{2-}$, Pd^{2+}, *etc.*) (Scheme 1b).[18–21] For instance, using $HAuCl_4$ as an oxidizing agent for the polymerization of pyrrole can lead to the simultaneous formation of very fine Au NPs in the core–shell metal–polymer nanocomposites.[22,23] Through an interfacial polymerization technique, Au–PANI nanocomposites can be obtained through the polymerization of aniline by $HAuCl_4$.[24] At low temperature, varying the concentration and molar ratio between aniline and $AuCl_3$ leads to a series of Au–PANI nanocomposites with a wide range of morphologies from nanosphere, nanorod, to complex nanosheet assemblies.[25] Au–PEDOT nanocomposites can be achieved by a one-step synthesis using $HAuCl_4$ as the oxidant to polymerize 3,4-ethylenedioxythiophene.[26,27] Polymerization of 3,5-dimethyl aniline

Hsing-Lin Wang

Hsing-Lin Wang was born in Taiwan. He received a BS degree in Chemistry (1984) from National Chung-Hsing University (Taiwan) and a PhD degree in Organic Chemistry (1992) from the University of South Florida. He then became a Postdoctoral Fellow at the University of Pennsylvania from 1993 to 1995 (with Prof. Alan G. MacDiarmid). He came to Los Alamos National Laboratory (LANL) as a Postdoctoral Fellow in 1995 and became a Technical Staff Member in 1998. He is now a senior scientist and project leader at LANL. His is the recipient of R&D 100 awards, NASA Cross Enterprise Technology Development Program Award and LANL Distinguished Performance Award. His research interests include development of conjugated polymers and their nanocomposites toward sensing, opto-electronic, and energy applications.

using Pd-acetate as the oxidant leads to a metal–polymer composite material, with Pd NPs (~2 nm) uniformly distributed throughout the polymer matrix.[21]

Therefore, synthesis of CP–MNP nanocomposites can be achieved through two reaction pathways. One involves the direct reduction of cations (Ag^+, Au^{3+}, Pd^{2+}, Pt^{2+}, *etc.*) by the CP powder or films (Scheme 1a), and the other pathway involves the chemical oxidation of monomers by metal salts (Scheme 1b). The advantages of this CP-mediated synthetic platform can be summarized as follows: (1) it is cost-effective and environmentally benign as no organic solvents, reducing agents, and polymer capping agents or surfactants are required, as compared to the conventional solution chemistry routes; (2) it allows facile control over the size, morphology and structure of the MNPs by adjusting the surface chemistry and redox properties of the CPs; and (3) it is a one-step reaction procedure leading to CP–MNP nanocomposites with collective properties pertaining to the two components. The CP–MNP nanocomposites can be used as effective surface enhanced Raman scattering (SERS) substrates for chemical detection, as highly efficient heterogeneous catalysts for organic synthesis and electrochemical reactions, and also as active components in electronic and memory devices.

In this tutorial review, we mainly focus on the designed synthesis and controlled functionality of polymer–metal nanocomposites through a direct chemical reduction of metal ions by CPs or chemical oxidation of monomers by metal salts. We begin with a brief introduction to the chemical nature and redox properties of CPs that enable spontaneous reduction of noble metal ions. We then demonstrate the recent progress in controlling the size, morphology and structure of nanocomposites by tailoring the surface chemistry of CPs. Finally, we present several examples to highlight the catalytic, sensing, and electronic properties of the polymer–metal nanocomposites.

2. Size, morphology and structure control of MNPs during CP-mediated synthesis

In conventional solution-phase synthesis, capping agents and surfactants are widely used to induce the anisotropic growth to control the size and morphology of MNPs.[1] Chemical reduction of metal ions by CPs relies on the surface chemistry of CPs, and the MNPs are either immobilized on CP surfaces or embedded within CP matrices. Therefore, in this heterogeneous growth process, capping agents and surfactants are usually not used to control the size, morphology and structure of the MNPs. However, there is a wide range of experimental parameters that one can vary to manipulate the size and morphology of the MNPs through the CP mediated synthesis.

2.1 Structure evolution of MNPs on CP surfaces

Taking the Ag deposition on PANI surfaces for example, a closer inspection of individual nucleation sites during different growth stages reveals detailed aspects of the CP-mediated deposition mechanism (Fig. 3a).[28] It is found that the initial nanoscale Ag particles consist of a few nanosheets clustered around one nucleation site. New nanosheets are then added to the nucleation site in a repeating random pattern. This unique growth process results from repetitive dissection of individual oblate Ag particles. Preferential deposition at the edges of the oblate structures leads to thin nanosheets. As new Ag^+ ions are reduced and added to the sheets, they proceed to ripen and eventually split into multiple new Ag sheets. Finally, Ag microspheres comprised of numerous nanosheets are formed. The growth mechanism of such Ag particles can be explained by the diffusion-limited aggregation (DLA) models as well as surface adsorption and reaction kinetics (Fig. 3b).[28] In a DLA regime, the sticking coefficient of new Ag onto the nucleation site is large and isotropic across the Ag surface, leading to highly branched fractal forest structures assuming Brownian diffusion (Fig. 3b, I); therefore, SEM images of these Ag particles display fractal branching structures with a clear preference for nanosheet growth, which implies that Ag^+ ions deposit on the PANI surface according to a DLA model but in a highly anisotropic fashion at the nucleated Ag surface, where the sticking coefficient at the edges of the oblate sheet structures is higher than that on the faces. In this semifractal growth regime, anisotropic deposition of newly formed Ag occurs on these reactive Ag crystal faces, resulting in highly branched nanosheet crystallites. In contrast, the addition of new Ag^+ ions to the metal surface is dictated by surface reaction kinetics and energetics when the sticking coefficient is low; in this case, a simple reduction of the Ag^+ ions at the Ag surface is presumed to be extremely fast and isotropic, leading to structures dominated by isotropic surface growth (Fig. 3b, II). These two growth regimes are very sensitive to temperature and ion concentration and provide unique opportunities to manipulate the overall Ag particle morphology.[28]

One of the main objectives of this tutorial review is to clearly demonstrate ways to control the size, structure and morphology

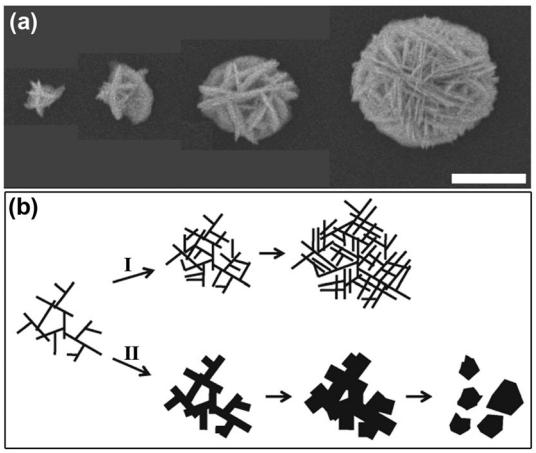

Fig. 3 (a) SEM images of Ag particles grown on citric acid doped PANI membranes at different reaction stages (scale bar: 1 μm). (b) Alternative growth modes for Ag particles on the PANI surface (I: diffusion-limited aggregation (DLA) fractal growth; II: surface growth). Adapted from the American Chemical Society.[28]

of MNPs spontaneously deposited on the CP surface. Systematic studies have been carried out to understand how experimental parameters impact the growth of MNPs, which are summarized as follows.

2.2 Effect of dopant of CP

The chemical nature and electrical conductivity of CPs can be easily tuned by the doping–dedoping treatments, which provide avenues to control the size and morphology of MNPs fabricated on CPs. For instance, the morphology of the Ag particles chemically deposited on PANI surfaces can be easily tuned by varying the doping acids for PANI membranes (Fig. 4).[29] As can be seen, chemical reduction of Ag^+ ions by PANI doped with HCl, citric acid, mandelic acid, toluenesulfonic acid, trifluoroacetic acid, and HBF_4 leads to Ag particles with random morphology, yarn-ball structures, nanosheet assemblies, nanowires, leaf-like structures, and chip structures, respectively. The above results clearly reveal the effect of doping acids on the size, morphology and structure of the chemically deposited MNPs.

Metal deposition on the CP membrane surfaces through this direct chemical reduction requires electron transfer from PANI to metal ions (see Scheme 1). When the metal ions approach the PANI surfaces, they are reduced by PANI and form nuclei. In a homogeneous system, where metal ions and the reducing agent are dispersed in solution, the metal nuclei serve as catalytic sites for surface growth, allowing the formation of larger metal structures.[1] However, in this heterogeneous system which involves PANI membranes, the growth mechanism differs from that of the homogeneous systems. The structure of metal nuclei is likely to be dominated by the difference in reduction potential (E^0) between metal ions and PANI, and by the surface properties of the PANI substrates. The morphological differences corresponding to various dopants may be due to the surface energy of the membrane which is dominated by the nature of the dopants and the redox states of the PANI membrane. The dopants may also change the interchain spacing of PANI, which could favor the growth of metal along a specific direction if the lattice parameters match the interchain distance.

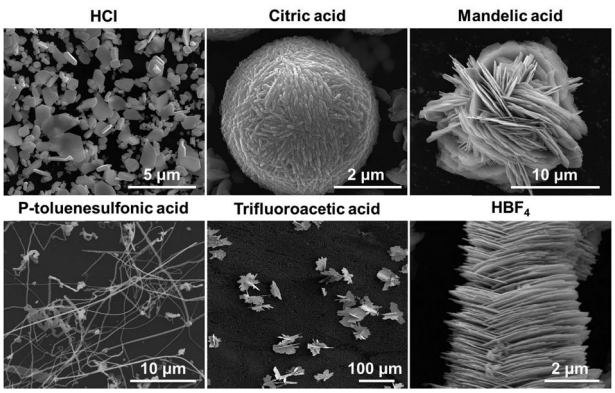

Fig. 4 SEM images of Ag structures grown on PANI surfaces doped with various acids through direct chemical reduction of Ag^+ ions by PANI. Adapted from the American Chemical Society.[29]

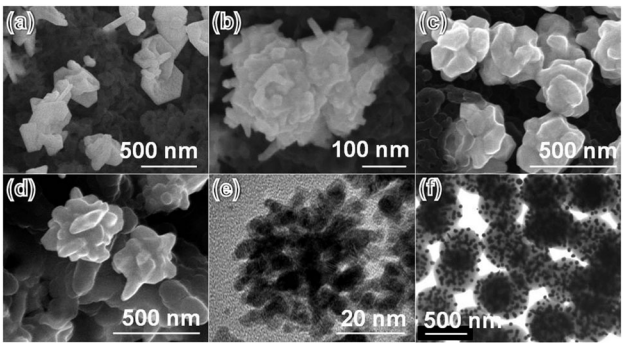

Fig. 5 Au nanostructures produced from chemical reduction by CPs with different compositions: PANI–PPy nanofibers with [An/Py] = 1 : 1 (a), 1 : 3 (b), 1 : 9 (c); PPy nanofibers (d) and nanospheres (e); and water soluble PEDOT : PSS (f). Adapted from Elsevier, Wiley-VCH, and American Chemical Society.[15–17,30]

2.3 Effect of CP composition

The composition of the CPs can also affect the size and morphology of chemically deposited MNPs. For example, on the PANI–PPy copolymer nanofibers prepared from different molar ratios of aniline and pyrrole [An/Py], one can get Au nanostructures with different sizes and morphologies.[15] Sphere-like Au nanostructures (50–100 nm) were produced on PANI–PPy nanofibers with [An/Py] = 9 : 1 and 3 : 1. Hexagonal Au nanosheets were deposited on the PANI–PPy nanofibers with equimolar An and Py (Fig. 5a). Chemical reduction of $AuCl_4^-$ ions by PANI–PPy nanofibers with [An/Py] = 1 : 3 and 1 : 9 yielded interesting sub-micron Au particles, where the former ratio led to chrysanthemum-shaped Au nanostructures comprised of Au NPs and nanorods, and the latter formed pinecone morphologies through self-organization of Au NPs (Fig. 5b). It is believed that PANI–PPy nanofibers with different compositions present surface property and reduction potential differences, leading to changes in the size and morphology of MNPs. The effect of CP composition is also manifested in the morphology of Au NPs chemically deposited on PPy,[16] as Au NPs deposited on PPy nanofibers present distinct differences from those obtained on PANI–PPy nanofibers. Moreover, it has been found out that the morphology of PPy (nanosphere *vs.* nanofiber) can result in morphological differences in the chemically deposited Au nanostructures (Fig. 5c and d), presumably due to the effective surface area accessible to the electrolytes and charge density on the PPy surface. What's more, the presence of a more negative reduction potential of PPy nanofibers than that of nanospheres may also contribute to the morphological differences of the Au NPs.[16] Reaction of $HAuCl_4$ with a water soluble conjugated polymer, PEDOT:PSS, led to scattered Au NPs or Au NP clusters, depending on the concentration of the $HAuCl_4$ solution (Fig. 5e).[17] Reduction of $HAuCl_4$ by poly(*o*-phenylenediamine) (P*o*PD) microspheres led to Au NPs with concentration-dependent particle size (Fig. 5f).[30]

2.4 Effect of CP substrate structures

Another parameter that can lead to morphology and structure variations of MNPs deposited on CPs is the physical structure of

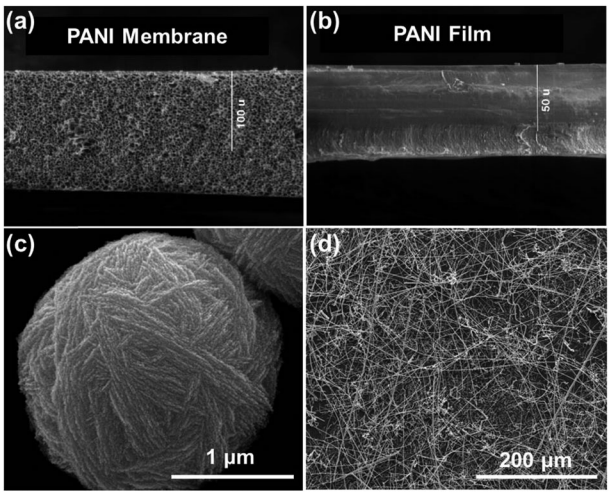

Fig. 6 SEM images of the cross section of a PANI membrane (a) and film (b), and Ag structures grown on a membrane (c) and film (d) doped with citric acid under identical conditions. Adapted from the American Chemical Society.[29]

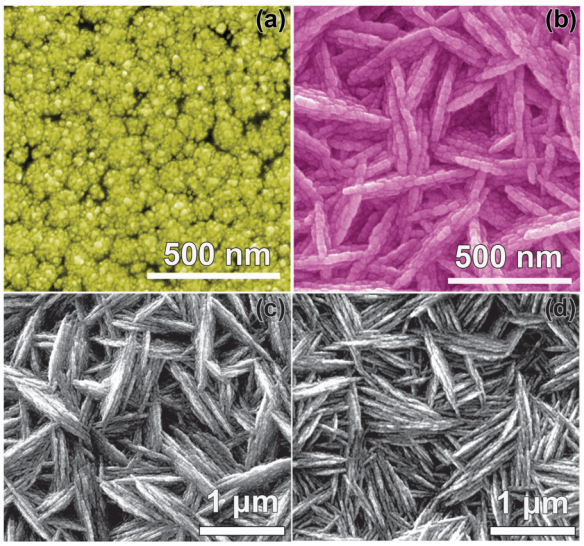

Fig. 7 SEM images of (a) Au NPs grown on a PANI membrane (doped with citric acid) by immersing the PANI membrane in 10 mM $AuCl_3$ aqueous solution for 10 s, (b) 3D Ag nanostructures produced by immersing the Au nanolayer-supported PANI membrane in 50 mM $AgNO_3$ aqueous solution for 60 min, and Ag nanostructures obtained by directly immersing the PANI–graphite (5 wt%) substrates doped with citric acid in (c) 50 and (d) 100 mM $AgNO_3$ solution for 30 min. Scale bar: 1 μm. Adapted from the Royal Society of Chemistry and American Chemical Society.[31,34]

the CP substrates. Depending on the post-treatment methods, PANI substrates with various structures can be obtained from highly concentrated PANI solution in *N*-methyl-2-pyrrolidone (NMP).[31] PANI membranes with porous sub-structures are produced by directly immersing the wet solution layer in water (Fig. 6a) to render a phase inversion process—solvent exchange between water and NMP. On the contrary, one can get PANI dense (non-porous) films when the solvent in the casted polymer wet film is thermally evaporated (Fig. 6b).

MNPs can be chemically deposited on the surface (skin layer) of the PANI porous membrane and dense film. When immersed in the same metal ion solutions, MNPs with dramatically different morphologies can be obtained. Yarn-ball like Ag structures comprised of numerous nanosheets are grown on the PANI membrane (Fig. 6c). A close inspection of these nanosheets reveals that they are indeed formed by an ensemble of even smaller Ag NPs. Interestingly, Ag nanowires with various detailed structures have been obtained on PANI dense films (Fig. 6d).[32] This morphological difference may have resulted from the difference in surface chemistry and doping level of the PANI substrates. Another interesting result we observed is that when we mechanically compressed the PANI membrane into a densely packed substrate using a hydraulic press, with a net effect of an increase in the overall density of the membrane and hence the relative number of nucleation sites on the PANI surface, complete surface coverage of Ag nanosheet structures is observed.[28,33] It is believed that the change in the volume density of the PANI membrane significantly alters the relative concentration of nucleation sites on the polymer surface. The increase in the density of nucleation sites by mechanical pressing of the PANI membranes allows neighboring MNPs to merge with each other and completely cover the surface with continuous and homogeneous Ag nanostructures.

2.5 Effect of conductivity of CP substrates

Though metal nanostructures can be readily grown on the CP surfaces based on the redox chemistry of CPs, as shown in Fig. 4–6, only scattered and sparsely populated particles are produced. For practical application purposes, CP substrates that are fully covered by homogeneous metal nanostructures are highly desired. Chemical reduction by CPs requires electron transfer from the CP matrix to the metal ions, and thus facilitating the electron transfer process may influence the nucleation and growth of metal nanostructures on the CP surfaces.

Through a two-step reaction route, pre-deposition of a Au nanolayer and subsequent growth of Ag nanostructures, with both steps utilizing the redox feature of PANI, homogeneous Ag nanosheet assemblies with well-defined 3D structures are achieved (Fig. 7a and b).[31] A close look reveals that the Ag nanosheets are comprised of an ensemble of tiny Ag NPs (Fig. 7b), similar to the nanosheets on the yarn-ball like Ag structures (Fig. 6c). A comparison between these two structures clearly indicates that the Au nanolayer acted as an electron conduit in the subsequent reduction of Ag^+ ions by PANI, which assists electron transfer from the PANI membranes and provides more nucleation sites for the fabrication of PANI substrates that are fully covered by Ag structures.

The effect of conductivity of CP substrates on the morphology of the fabricated metal nanostructures can also be manifested by addition of conductive carbon nanotubes (CNTs) or graphite into the CP substrates.[33] Direct immersion of citric acid doped PANI-CNT membranes (replacing 5 wt% PANI with CNTs) in $AgNO_3$ solution with concentrations higher than 15 mM leads to homogeneous Ag nanostructures fully covering the membrane surface. Low-cost graphite can play the same role as the expensive CNTs, as similar homogeneous Ag nanostructures can be obtained on PANI–graphite surfaces (Fig. 7c and d). A close

examination of these nanosheets, following the nanosheet growth as a characteristic of using citric acid as the doping agent, reveals that they are formed by an ensemble of ~20 nm Ag NPs, indicating that the conductive additives will not change the growth nature of the Ag nanostructures. However, with densely populated nucleation sites and a facile charge transfer process induced by the conductive additives, homogeneous nanosheet assemblies spreading over the substrate surface are achieved instead of close packed microspheres.

2.6 Effect of acid-directed growth

Another effective route to control the size and morphology of the metal nanostructures supported on CP surfaces lies in the acid-directed growth process,[35] which actually makes the fabrication of homogeneous metal nanostructures even more simple and cost-effective.

It has been shown that homogeneous Ag nanostructures fully covering the substrate surfaces can be readily obtained by immersing the doped PANI membranes in the $AgNO_3$ solution with a small amount of acid additive (Fig. 8a). This process appears very attractive as no pre-fabrication of Au nanolayers or conductive additive is required, which is time- and cost-effective. However, this acid-directed technique did not work on undoped PANI surfaces, as shown in Fig. 8b, where only scattered Ag particles were deposited. One possible reason is the restrained charge transfer process and limited nucleation sites in the undoped substrates. Moreover, the difference in surface wettability of the doped and undoped PANI membranes may also contribute to the nucleation and growth of metal nanostructures on CP (Fig. 8c and d). Improved wettability of the doped PANI membrane allows a favorable interface interaction

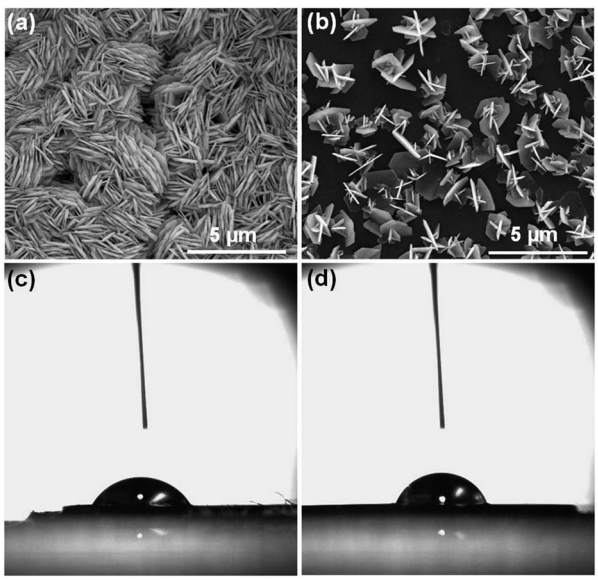

Fig. 8 SEM images of Ag nanostructures grown on camphorsulfonic-acid-doped (a) and undoped (b) PANI membranes, with succinic acid present in the $AgNO_3$ solution. Surface wettability comparison of doped (c, contact angle = 60.1°) and undoped (d, contact angle = 72.3°) PANI membranes. Adapted from the American Chemical Society.[35]

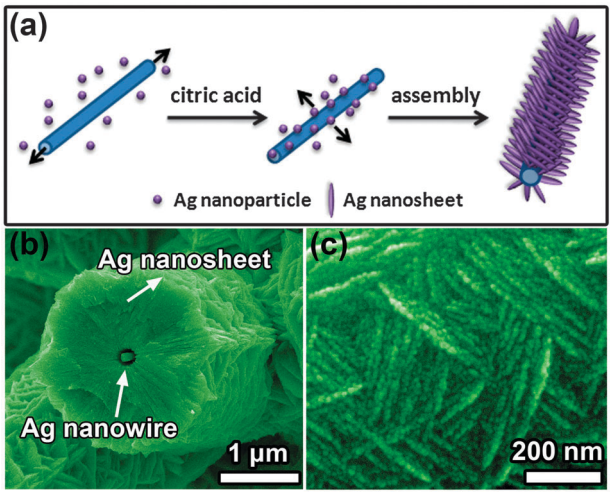

Fig. 9 Schematic illustration of the acid-directed synthesis (a) and SEM images (b) and (c) of the core–shell Ag wires on citric acid doped PANI films. Adapted from the Royal Society of Chemistry.[36]

with Ag^+ ions and thus facilitates the formation of a higher surface coverage of Ag nanostructures. A careful look at these Ag structures reveals that they are also formed by an assembly of Ag nanosheets. However, the Ag nanosheets here are smooth polygons, clearly different from those obtained previously when using citric acid as the additive (formed by assembled Ag NPs). We believe that such difference may have resulted from the acid effect, which dictates the Ag growth mechanisms.

This acid-directed growth mechanism can be further adapted to fabricate core–shell Ag–Ag wire structures on the PANI films. As shown in Fig. 9a and b, during the Ag nanowire growth on PANI films, addition of citric acid will direct the newly formed Ag NPs assemble on the nanowire and lead to core–shell wire structures.[36] The Ag nanosheet assemblies that form the shell are actually comprised of numerous Ag NPs (Fig. 9c), similar to those found on the yarn-ball like Ag structures on PANI membranes (Fig. 6c). The formation mechanism of such core–shell structures was revealed by a time-dependent SEM study, which involved an initial growth of Ag NPs on the nanowire, and then expansion into assembled nanosheet structures. These results indicate that acid molecules adsorbed on the Ag nucleates can direct the ensuing Ag growth by way of self-assembly, which has been found to be effective in the fabrication of hierarchical Ag structures via a solution chemistry route.[36]

2.7 Other factors

Other experimental parameters that can change the size, morphology and structure of MNPs through direct chemical reduction by CPs include the metal ion concentration, reaction temperature, the applied electric field, and additives introduced into the metal ion solution.[28,37–39] This review in no way suggests the exhaustion of experimental factors and fabrication techniques that can control the size and morphology of MNPs through the CP mediated synthesis methodology. Yet, the existing findings have revealed an exciting and interesting synthetic platform to synthesize MNPs with controlled

size, morphology and structure that are not accessible through conventional solution chemistry methods.

3. Applications of CP–MNP nanocomposites

The ease of using the redox chemistry of CPs to chemically deposit MNPs on CPs has enabled a wide range of applications of the polymer–metal nanocomposites, which present synergetic properties of the conductivity of CPs and the optical, catalytic and electronic properties of MNPs. Herein, we mainly focus on their applications as SERS-active materials for chemical detection, heterogeneous catalysts for organic synthesis and electrochemical reactions, and key components for electronic and sensing devices.

3.1 SERS-active materials for molecular detection and sensing

SERS, mainly utilizing the greatly enhanced electromagnetic field and the localized surface plasmon resonances generated at the metal surfaces upon laser excitation to enhance the Raman signal of an analyte up to a dozen orders of magnitude, has been recognized as a powerful tool for chemical analysis and sensing applications.[40] However, as SERS hot spots—locations with extremely strong SERS response—are usually located at the interstitial sites (intersections, bifurcations, and high radius of curvatures) in nanostructures, individually dispersed NPs only provide very limited Raman enhancement. Controlled synthesis of SERS active materials with densely populated and homogeneously dispersed "hot spots" is very challenging, as it requires exquisite preparation of MNPs with certain size and morphology and delicate manipulation of the NP assemblies.[31] Though a number of promising silver structures have been found to be efficient SERS-active platforms, fabrication of highly sensitive and reproducible SERS substrates remains a great challenge. The resultant nanocomposites derived from the chemical deposition of homogeneous MNP on CP have shown great promise as highly efficient and cost-effective SERS platforms for chemical detection (Fig. 10a).

The nanocavities formed by the Ag nanosheet stacks and the junctions and gaps between two Ag NPs from the Ag nanostructures as shown in Fig. 7b serve as effective SERS hot spots. Using 4-mercaptobenzoic acid (4-MBA) as a target analyte, the homogeneous Ag nanosheet assemblies with well-defined 3D structures show strong and uniform SERS response over a large area with an average enhancement factor of 10^6–10^7 (Fig. 10b).[31] Remarkably, SERS activity of the assembled Ag nanosheet structure shown in Fig. 8a is extremely high, where 4-MBA with a concentration of 10^{-12} M can be easily tracked (Fig. 10c).[35] Notably, the fabricated core–shell Ag wires show extremely high SERS activity toward melamine, with a detection sensitivity of 5 ppm (Fig. 10d).[36] The high sensitivity and efficiency of using CP-based metal nanostructures as SERS platforms mainly rely on the homogeneous coverage and morphological features of the as-fabricated MNPs that offer numerous SERS hot spots over a large area. It is worth noting that these CP-based substrates are more convenient and inexpensive to make, as compared to the state-of-the-art lithography-based SERS substrates. Recent studies have shown that treating the PANI substrate with hydrazine, which renders PANI with an even lower reduction potential, can accelerate the Ag growth and provide a way for fast fabrication (within several minutes) of SERS-active substrates.[41] Using ascorbic acid, an intrinsic reducing agent for synthesizing MNPs, as the dopant of PANI substrates can also facilitate the MNP growth.

Besides Ag, thorny Au nanostructures can also be fabricated through the CP-mediated technique at an elevated temperature of 80 °C (Fig. 11a).[39] The size of the nanoneedles on the thorny structures can be controlled by the reaction time. Those thorny Au nanostructures, with higher surface areas and unique geometric features, show a SERS detection sensitivity of 10^{-9} M (sub-ppb level) toward two different analyte molecules (Fig. 11b), 4-MBA and Rhodamine B, demonstrating their generality for SERS applications. This is the first example of SERS-active Au nanostructures fabricated on PANI substrates with such a high sensitivity.

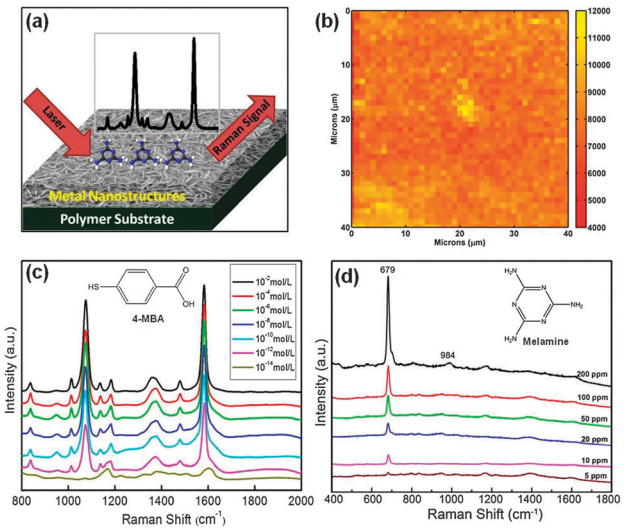

Fig. 10 (a) Schematic illustration of using the MNPs immobilized on CP substrates as highly sensitive SERS platforms, (b) Raman mapping of the 1080 cm^{-1} band of 4-MBA on the substrate shown in Fig. 7b, (c) concentration-dependent SERS spectra of 4-MBA on the substrate shown in Fig. 8a, and (d) concentration-dependent SERS spectra of melamine on the core–shell Ag wire structures shown in Fig. 9. Adapted from the American Chemical Society and the Royal Society of Chemistry.[31,35,36]

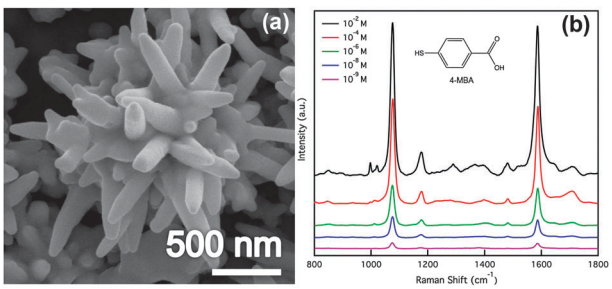

Fig. 11 SEM images of thorny Au nanostructures fabricated on the PANI membrane (a) and SERS response toward the analyte 4-MBA (b). Adapted from the American Chemical Society.[39]

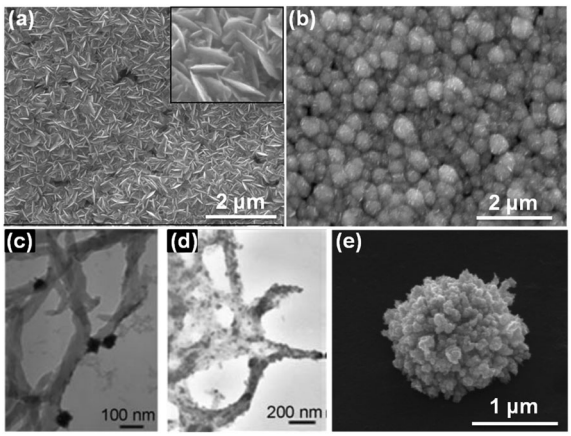

Fig. 12 SEM images of Pd nanostructures formed by direct chemical reduction on an undoped PANI membrane (a) and a thermally cured PANI dense film (b). TEM images of Pd NPs supported on PANI nanofibers (c), and the catalyst after two cycles (d). SEM image of Pt nanostructures formed on doped PANI membranes (e). Adapted from the American Chemical Society and Wiley-VCH.[43–45]

3.2 Efficient heterogeneous catalysts for organic synthesis and electrochemistry

Conventional heterogeneous noble metal catalysts typically involve Pt, Pd or Au NPs supported on carbon materials. MNPs supported on CPs have been the subject of interest as they represent a new class of efficient heterogeneous catalysts. These as-fabricated polymer–metal nanocomposites have been used as efficient heterogeneous catalysts for organic synthesis and electrocatalytic reactions. For example, PANI–Pt nanocomposites prepared by the spontaneous reduction of K_2PtCl_4 with PANI were processed into thin films that show electrocatalytic properties in both acidic and neutral aqueous media.[42]

Evenly distributed Pd nanostructures were spontaneously deposited on PANI surfaces through an *in situ* reduction of $Pd(NO_3)_2$ by PANI.[43] The size and morphology of the Pd NPs are dependent on the nature of the substrate surfaces: Pd particles on the PANI membrane have a sheet-like rough surface morphology with a size distribution of ~200 nm (Fig. 12a), and those on the PANI dense film have a smooth surface with a size distribution of ~500 nm (Fig. 12b). Pd NPs exhibit efficient catalytic activity toward hydrogenation of alkynes and cinnamaldehyde with high selectivity dominated by a kinetic mechanism. Moreover, the variation in Pd particle morphology leads to differences in their catalytic efficiency presumably due to the difference in surface area. Considering the hydrogenation reaction of cinnamaldehyde as an example (Scheme 2), it was revealed that under a catalyst loading of 5 mol%, PANI-supported Pd catalysts exhibit a high selectivity toward the formation of hydrocinnamaldehyde (**I**). However, the obtained Pd structures on membranes or films can severely affect the conversion ratio. After 28 h, a conversion ratio of 100% is reached by using Pd on PANI membranes, with 72% of **I** and 28% of 3-phenyl-1-propanol (**II**). With Pd on PANI films, a conversion ratio of only 35% was obtained even after 48 h, with 75% of **I** and 25% of **II**. The higher yield of **I** is extremely important as it is a precursor for the preparation of protease inhibitors used in the treatment of HIV. The PANI-supported Pd NPs are robust and can be reused at least seven times without a significant loss of its catalytic activity and selectivity. Pd NPs supported on PANI nanofibers have been used as active catalysts for Suzuki coupling between aryl chlorides and phenylboronic acid and for phenol formation from aryl halides and potassium hydroxide in water and air (Fig. 12c).[44] After using the catalyst for two cycles, no large Pd agglomerates are seen (Fig. 12d). The authors noticed a decline in the quality of the nanofiber support along with a change in the distribution of NP sizes that might be responsible for the decrease in yield over extended recycling.

The morphologies of Pt nanostructures deposited on PANI surfaces largely depend on the doping state of the membranes.[45] As shown in Fig. 12e, Pt aggregates that are assembled by smaller NPs are formed on the doped PANI membranes, as opposed to the sheet-like Pt structures deposited on undoped PANI membranes. This is another piece of evidence of the doping effect on the size and morphology of the chemically deposited MNPs on CP surfaces. Such morphological differences in Pt particles also have impacts on the catalytic performance of the polymer–metal nanocomposites. The regioselective hydrosilylation reactions of *para*- and *ortho*-substituted aryl alkynes (**1a**, **1b**) with Et_3SiH were selected as model catalytic reactions (Scheme 3). Interestingly, the relative catalytic efficiency of Pt particles on doped and undoped PANI is essentially identical, presumably because the NP size and the surface morphologies are comparable in relation to the size of the catalytically active sites on the Pt metal surface. Both **1a** and **1b** were completely converted to greater than 83% enantiomeric excess of the α-isomer with a combined yield of greater than 95%, without the formation of *Z* + *E*. Although the reaction rate is relatively slow as compared to that obtained with the commercial Pt/C catalyst, the Pt/PANI materials exhibit enhanced regioselectivity and improved yields.

As noted previously, Au NPs immobilized on CPs can be manufactured through (i) chemical reduction of Au^{3+} ions by CP and (ii) polymerization of monomers by Au^{3+} ions. For the first synthetic route, thioglycolic acid (TA) introduced in PANI nanofibers shows improved uniformity of composites and control over Au NP size (Fig. 13a).[37] PANI nanofiber/Au nanocomposites are found to serve as effective recycled catalysts for

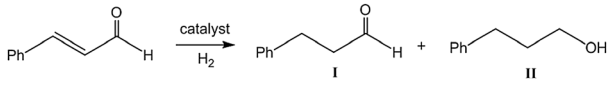

Scheme 2 Schematic illustration of the hydrogenation reaction of cinnamaldehyde using PANI-supported Pd catalyst. **I** and **II** are the possible products, and the reaction conditions are a pressure of ~1 atm and room temperature.

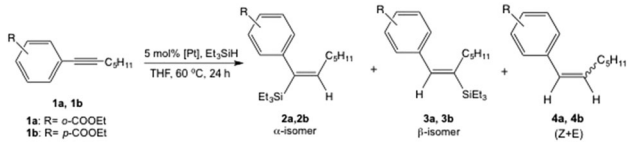

Scheme 3 Schematic illustration of the hydrosilylation reactions of internal *para*- and *ortho*-substituted aryl alkynes on PANI supported Pt.

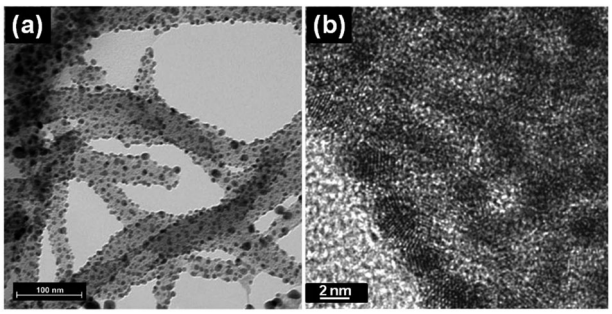

Fig. 13 TEM images of (a) Au NPs supported on PANI nanofibers using PANI as both the supporter and reductant, and (b) Au–PANI nanocomposites prepared from an interfacial polymerization of aniline by $HAuCl_4$. Adapted from the American Chemical Society and Royal Society of Chemistry.[24,37]

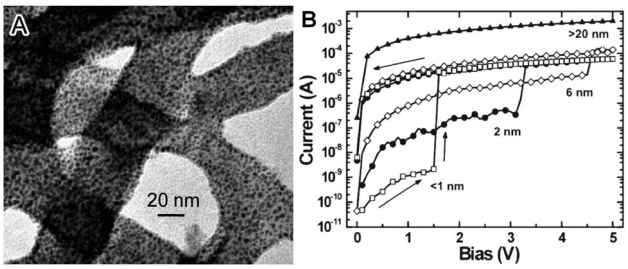

Fig. 14 (A) TEM image of a PANI–Au nanocomposite prepared by exposure of PANI nanofibers to $HAuCl_4$ under controlled conditions; (B) Au NP size-dependent characteristic *I*–*V* scans for Au NP–PANI nanofiber composite memory devices in which the composite is sandwiched by two Al electrodes. Adapted from the American Chemical Society.[48,49]

the reduction of 4-nitrophenol (4NP) in the presence of $NaBH_4$, where the size of Au NPs is found to play a dominant role in catalytic activity. The second synthetic route can be reflected in an interfacial polymerization route to synthesize Au–PANI nanocomposites *via* polymerization of aniline by $HAuCl_4$,[24] with highly crystallized Au NPs (2–3 nm in diameter) embedded in the PANI nanospheres (Fig. 13b). The as-prepared Au–PANI nanocomposites are efficient catalysts for the reduction of Rhodamine B by $NaBH_4$, where complete conversion of Rhodamine B is reached in just several minutes. Poly(*o*-phenylenediamine) (P*o*PD) submicrosphere-supported Au nanocatalysts can also be prepared *via* the chemical reduction of $HAuCl_4$ by P*o*PD, which can be applied to the selective oxidation of benzyl alcohol.[30] Highly uniform self-assembled poly(2-aminothiophenol) (PATP)–Au fibrous nanocomposites have been synthesized from the polymerization of 2-aminothiophenol monomers by $HAuCl_4$, which are efficient recyclable catalysts for the reduction of 4NP by $NaBH_4$.[46] CP–MNP nanocomposites involving Pt or Pd NPs are effective electrocatalysts. *In situ* reduction of K_2PtCl_4 by PANI in a variety of solvents results in Pt NPs and clusters of different sizes.[47] Pt clusters can also be deposited on PANI–Pt nanocomposite thin films from a neutral aqueous solution of K_2PtCl_4. Thin-film electrodes prepared from these materials have been investigated for their electrocatalytic activity for hydrazine oxidation and dichromate reduction.[47]

3.3 Key components for electronic and sensing devices

Incorporation of MNPs in CPs can enhance electron transfer through a direct or mediated mechanism due to improved conductivity and enhanced stability. Therefore, besides their successful applications as SERS-active materials for chemical detection and as efficient heterogeneous catalysts for organic synthesis and electrocatalysis, CP–MNP nanocomposites can also function as key components for electronic and sensing devices.

As shown in Fig. 14A, PANI nanofibers decorated with Au NPs through chemical reduction of $HAuCl_4$ by PANI as an active layer sandwiched between two aluminum electrodes possess a remarkable electrically switchable bistability, which is ideal for nonvolatile flash memory devices.[48] By controlling the size of the Au NPs grown on PANI nanofibers at $\sim$2 nm, the device can be switched from the off- to the on-state at $\geq$3 V with a switching time of $\leq$25 ns, which produces an abrupt increase in current of more than 3 orders of magnitude and can be switched back to the off-state at less than or equal to -5 V (Fig. 14B). This device is stable in both states and switching between these two states can be repeated numerous times without any obvious decay. It has been confirmed that both PANI and Au NPs are important for the device, as absence of either component will simply lead to the disappearance of the bistable switching behavior. Switching properties of the nanocomposite originate from an electric field induced charge transfer between PANI nanofibers and Au NPs, and the charges can be stably trapped on the Au NPs even when the applied electric field is removed. Both the charge transfer and stability of the device are dependent on the nanoscale dimensions of both component materials and the interface formed between Au NPs and PANI nanofibers.

The effect of the Au NP size on the memory device performance has also been studied using Au NPs with four distinct sizes ($<$1, 2, 6, and $>$20 nm) (Fig. 14B).[48] As can be seen, the turn-on voltages of the devices fabricated with $<$1, 2, and 6 nm Au NPs are 1.5, 3, and 4.5 V, respectively, and the on/off ratio (difference between the low conductivity state and high conductivity state measured at 1 V) is 4, 3, and 1.5 orders of magnitude, respectively. Notably, the device with $>$20 nm Au NPs did turn on once during the first scan, with a turn-on voltage of 6 V. However, this device cannot be erased and just remains in its high conductivity state after the first scan, presumably due to shorting of the device from filament formation and/or agglomeration of the relatively large Au NPs. An ideal device should have a larger on/off ratio to provide more stability and a lower turn-on voltage to consume less power. The lower turn-on voltages with smaller Au NPs may be attributed to a decreased barrier from the close proximity of the Au NPs. Therefore, best device performances are obtained from Au–PANI nanocomposites with 2 nm Au NPs, with the advantages of low turn-on voltage, large on/off ratio, and best cycling ability (can undergo $>$100 write–read–erase cycles).

Another potential implication of CP–MNP nanocomposites is in the area of chemical sensing using electrical and optical

responses as transduction signals. So far, there are only scattered reports of using CP–MNP composites fabricated from chemical deposition as effective chemical sensors. For example, using 3-aminophenylboronic acid (3-APBA) as both the reductive and protective agent in the presence of $HAuCl_4$, water-soluble Au–PAPBA nanocomposites were synthesized.[50] Poly(vinyl alcohol) (PVA) was used as a steric stabilizer based on the covalent bond formation between the boronic acid and the diol group. The as-prepared nanocomposite could be used as a sensitive optical probe for the detection of glucose.[50]

4. Concluding remarks

Noble metal nanoparticles (MNPs) such as Ag, Au, Pt and Pd have received continuous interest due to their promise in catalysis, electrocatalysis, sensing, and imaging applications. However, most chemical routes to synthesize MNPs require organic solvents and polymer capping agents in order to achieve control over size, morphology and structure of the nanocrystals, which are considered environmentally unfriendly and cost ineffective. Recent studies have revealed a reliable alternative method—direct synthesis of MNPs *via* the conjugated polymer (CP) mediated chemical reduction methodology. This method has received a great deal of attention owing to its spontaneous formation of multifunctional CP–MNP nanocomposites. To date, Ag, Au, Pt and Pd NPs have been successfully synthesized through this CP mediated synthesis technique. MNPs with a wide range of size, structure, and morphology have been fabricated by varying the experimental parameters such as doping state, composition, substrate structure, conductivity, ion concentration, reaction temperature, and additives introduced into the metal ion solution. The as-fabricated CP–MNP nanocomposites have been explored as multifunctional materials for practical applications. Ag and Au nanostructures fabricated on PANI substrates (membrane and film) show promising applications as highly sensitive SERS platforms for chemical detection. Pt, Pd and Au MNPs fabricated on PANI substrates and nanofibers have been identified as effective heterogeneous catalysts for organic synthesis, dye degradation and electrochemical reactions. Moreover, the Au NPs chemically deposited on PANI nanofibers have been used in bistable nonvolatile memory devices and glucose sensors.

The CP–MNP nanocomposites described in this tutorial review mainly take advantage of one polymer from the CP family, PANI. Other CPs and their derivatives, as displayed in Fig. 1, have demonstrated their feasibility for synthesizing nanocomposites through similar chemical reduction routes. However, functionalization of those products remains to be exploited, which may have even significant application potentials due to the varying chemical nature of different CPs.

Although significant progress has been made in the CP-mediated direct synthesis of MNPs, successful preparation of metal alloys is limited. Except for the formation of jellyfish-like Au–Ag alloy structures on PANI substrates through a sequential deposition technique,[34] other alloys like Pt–Pd, Pt–Au, and Pd–Au have not yet been achieved by the CP-mediated technique. As these bimetallic nanostructures can be applied as highly efficient electrocatalysts in fuel cells and batteries,[1] fabrication of nanostructured alloys using CP mediated synthetic platforms may lead to novel structures with emerging properties, which can further improve the catalytic efficiencies and performance characteristics of electronic and energy devices. As metal ions are reduced by CPs when they approach the polymer surface, this spontaneous chemical reduction and immobilization process may render stronger binding force between the MNPs and CP to achieve long-term durability as opposed to the commercial carbon-supported MNP catalysts. Therefore, we foresee CP–MNP nanocomposites have huge impacts on the development of future generation of energy devices such as fuel cells and lithium ion (lithium–air) batteries, as well as electronic and sensing devices.

Acknowledgements

PX acknowledges support from the China Postdoctor Fund, NSFC (Nos 21203045, 21101041, 21003029, 21071037, 91122002, 51377048), Fundamental Research Funds for the Central Universities (Nos HIT.NSRIF. 2010065 and 2011017, and HIT.BRETIII. 201223), the 9th Thousand Foreign Experts Program, and Director's Postdoctoral Fellow from LANL. Preparation of nanostructured metals for catalytic studies was supported by Basic Energy Science (BES), and Biomolecular Materials Program, Materials and Engineering Division. HLW acknowledges support from the Laboratory Directed Research and Development (LDRD) fund under the auspices of DOE.

Notes and references

1 H. Zhang, M. S. Jin and Y. N. Xia, *Chem. Soc. Rev.*, 2012, **41**, 8035–8049.
2 H. Lee, S. E. Habas, S. Kweskin, D. Butcher, G. A. Somorjai and P. D. Yang, *Angew. Chem., Int. Ed.*, 2006, **45**, 7824–7828.
3 B. Lim, M. J. Jiang, P. H. C. Camargo, E. C. Cho, J. Tao, X. M. Lu, Y. M. Zhu and Y. N. Xia, *Science*, 2009, **324**, 1302–1305.
4 J. Pecher and S. Mecking, *Chem. Rev.*, 2010, **110**, 6260–6279.
5 Q. Wu, Y. X. Xu, Z. Y. Yao, A. R. Liu and G. Q. Shi, *ACS Nano*, 2010, **4**, 1963–1970.
6 D. W. Hatchett and M. Josowicz, *Chem. Rev.*, 2008, **108**, 746–769.
7 J. Chen, J. Abell, Y. W. Huang and Y. Zhao, *Lab Chip*, 2012, **12**, 3096–3102.
8 V. Armel, O. Winther-Jensen, R. Kerr, D. R. MacFarlane and B. Winther-Jensen, *J. Mater. Chem.*, 2012, **22**, 19767–19773.
9 Y. P. Ting, K. G. Neoh, E. T. Kang and K. L. Tan, *J. Chem. Technol. Biotechnol.*, 1994, **59**, 31–36.
10 D. Li, J. X. Huang and R. B. Kaner, *Acc. Chem. Res.*, 2009, **42**, 135–145.
11 W. G. Li, Q. X. Jia and H. L. Wang, *Polymer*, 2006, **47**, 23–26.
12 V. Tsakova, D. Borissov, B. Ranguelov, C. Stromberg and J. W. Schultze, *Electrochim. Acta*, 2001, **46**, 4213–4222.

13 Y. Zhou, H. Itoh, T. Uemura, K. Naka and Y. Chujo, *Chem. Commun.*, 2001, 613–614.
14 Y. Zhou, H. Itoh, T. Uemura, K. Naka and Y. Chujo, *Langmuir*, 2002, **18**, 277–283.
15 P. Xu, X. J. Han, C. Wang, D. H. Zhou, Z. S. Lv, A. H. Wen, X. H. Wang and B. Zhang, *J. Phys. Chem. B*, 2008, **112**, 10443–10448.
16 P. Xu, X. J. Han, B. Zhang, N. H. Mack, S. H. Jeon and H. L. Wang, *Polymer*, 2009, **50**, 2624–2629.
17 P. Xu, K. Chang, Y. I. Park, B. Zhang, L. L. Kang, Y. C. Du, R. S. Iyer and H. L. Wang, *Polymer*, 2013, **54**, 485–489.
18 Y. C. Liu, *Langmuir*, 2002, **18**, 9513–9518.
19 X. H. Dai, Y. W. Tan and J. Xu, *Langmuir*, 2002, **18**, 9010–9016.
20 J. M. Kinyanjui, J. Hanks, D. W. Hatchett, A. Smith and M. Josowicz, *J. Electrochem. Soc.*, 2004, **151**, D113–D120.
21 K. Mallick, M. J. Witcomb, A. Dinsmore and M. S. Scurrell, *Langmuir*, 2005, **21**, 7964–7967.
22 S. T. Selvan, J. P. Spatz, H. A. Klok and M. Moller, *Adv. Mater.*, 1998, **10**, 132–134.
23 S. T. Selvan, *Chem. Commun.*, 1998, 351–352.
24 B. Zhang, B. T. Zhao, S. H. Huang, R. Y. Zhang, P. Xu and H. L. Wang, *CrystEngComm*, 2012, **14**, 1542–1544.
25 Y. F. Huang, Y. I. Park, C. Kuo, P. Xu, D. J. Williams, J. Wang, C. W. Lin and H. L. Wang, *J. Phys. Chem. C*, 2012, **116**, 11272–11277.
26 H. Mao, X. F. Lu, X. C. Liu, J. Tang, C. Wang and W. J. Zhang, *J. Phys. Chem. C*, 2009, **113**, 9465–9472.
27 X. H. Li, Y. C. Li, Y. W. Tan, C. H. Yang and Y. F. Li, *J. Phys. Chem. B*, 2004, **108**, 5192–5199.
28 N. H. Mack, J. A. Bailey, S. K. Doorn, C. A. Chen, H. M. Gau, P. Xu, D. J. Williams, E. A. Akhadov and H. L. Wang, *Langmuir*, 2011, **27**, 4979–4985.
29 H. L. Wang, W. G. Li, Q. X. Jia and E. Akhadov, *Chem. Mater.*, 2007, **19**, 520–525.
30 J. Han, Y. Liu, L. Y. Li and R. Guo, *Langmuir*, 2009, **25**, 11054–11060.
31 P. Xu, N. H. Mack, S. H. Jeon, S. K. Doorn, X. J. Han and H. L. Wang, *Langmuir*, 2010, **26**, 8882–8886.
32 P. Xu, S. H. Jeon, H. T. Chen, H. M. Luo, G. F. Zou, Q. X. Jia, M. Anghel, C. Teuscher, D. J. Williams, B. Zhang, X. J. Han and H. L. Wang, *J. Phys. Chem. C*, 2010, **114**, 22147–22154.
33 P. Xu, B. Zhang, N. H. Mack, S. K. Doorn, X. J. Han and H. L. Wang, *J. Mater. Chem.*, 2010, **20**, 7222–7226.
34 P. Xu, E. Akhadov, L. Y. Wang and H. L. Wang, *Chem. Commun.*, 2011, **47**, 10764–10766.
35 J. Yan, X. J. Han, J. J. He, L. L. Kang, B. Zhang, Y. C. Du, H. T. Zhao, C. K. Dong, H. L. Wang and P. Xu, *ACS Appl. Mater. Interfaces*, 2012, **4**, 2752–2756.
36 B. Zhang, P. Xu, X. M. Xie, H. Wei, Z. P. Li, N. H. Mack, X. J. Han, H. X. Xu and H. L. Wang, *J. Mater. Chem.*, 2011, **21**, 2495–2501.
37 J. Han, L. Y. Li and R. Guo, *Macromolecules*, 2010, **43**, 10636–10644.
38 P. Xu, S. H. Jeon, N. H. Mack, S. K. Doorn, D. J. Williams, X. J. Han and H. L. Wang, *Nanoscale*, 2010, **2**, 1436–1440.
39 S. W. Li, P. Xu, Z. Q. Ren, B. Zhang, Y. C. Du, X. J. Han, N. H. Mack and H. L. Wang, *ACS Appl. Mater. Interfaces*, 2013, **5**, 49–54.
40 F. Casadio, M. Leona, J. R. Lombardi and R. Van Duyne, *Acc. Chem. Res.*, 2010, **43**, 782–791.
41 J. J. He, X. J. Han, J. Yan, L. L. Kang, B. Zhang, Y. C. Du, C. K. Dong, H. L. Wang and P. Xu, *CrystEngComm*, 2012, **14**, 8737.
42 A. P. O'Mullane, S. E. Dale, J. V. Macpherson and P. R. Unwin, *Chem. Commun.*, 2004, 1606–1607.
43 Y. Gao, C. A. Chen, H. M. Gau, J. A. Bailey, E. Akhadov, D. Williams and H. L. Wang, *Chem. Mater.*, 2008, **20**, 2839–2844.
44 B. J. Gallon, R. W. Kojima, R. B. Kaner and P. L. Diaconescu, *Angew. Chem., Int. Ed.*, 2007, **46**, 7251–7254.
45 H. H. Shih, D. Williams, N. H. Mack and H. L. Wang, *Macromolecules*, 2009, **42**, 14–16.
46 J. Han, J. Dai, L. Y. Li, P. Fang and R. Guo, *Langmuir*, 2011, **27**, 2181–2187.
47 A. P. O'Mullane, S. E. Dale, T. M. Day, N. R. Wilson, J. V. Macpherson and P. R. Unwin, *J. Solid State Electrochem.*, 2006, **10**, 792–807.
48 C. O. Baker, B. Shedd, R. J. Tseng, A. A. Martinez-Morales, C. S. Ozkan, M. Ozkan, Y. Yang and R. B. Kaner, *ACS Nano*, 2011, **5**, 3469–3474.
49 R. J. Tseng, J. X. Huang, J. Ouyang, R. B. Kaner and Y. Yang, *Nano Lett.*, 2005, **5**, 1077–1080.
50 Y. Ma, N. Li, C. Yang and X. R. Yang, *Colloids Surf., A: Physicochemical and Engineering Aspects*, 2005, **269**, 1–6.

